MRS Advances
https://doi.org/10.1557/s43580-024-00790-8

ORIGINAL PAPER

A-site occupancy effects on structure, ionic conductivity, and thermodynamic stability of $K_xMg_{x/2}Ti_{8-x/2}O_{16}$

Nakeshma S. Cassell[1] · Nancy Birkner[1] · A. K. Mishra[1] · Shraddha Jadhav[1] · Amir M. Mofrad[2] · Theodore M. Bessmann[2] · Jake W. Amoroso[3] · Yuhan Li[4] · Lumin Wang[4] · Kyle S. Brinkman[1]

Received: 30 November 2023 / Accepted: 26 January 2024

Abstract

$K_xMg_{x/2}Ti_{8-x/2}O_{16}$ ($1.54 \leq x \leq 2$) hollandite samples synthesized using a conventional solid-state route were used to investigate the effect of structure, ionic conductivity, and thermodynamic stability as a function of A-site (K) occupancy. The ionic conductivity, as measured using AC impedance spectroscopy, decreased as the A-site occupancy (and K content) increased. Titanate hollandite, of the form $K_xMg_{x/2}Ti_{8-x/2}O_{16}$, was measured using high-temperature oxide melt solution calorimetry in sodium molybdate ($3Na_2O \bullet 4MoO_3$) solvent at 804 °C. The enthalpies of formation are strongly exothermic indicating that they are thermodynamically stable relative to their constituent oxides. Previous studies have demonstrated increased stability with an increase in Cs content at fixed A-site occupancy. This work demonstrated an increase in the stability for the K-bearing hollandite samples with an increase in K content and tunnel occupancy. The measured enthalpies of formation ($\Delta H_{f,ox}$) were in good agreement with density functional theory (DFT) predictions.

Introduction

The demand for clean energy has accelerated the development and design of new materials for use in energy systems including materials for nuclear waste immobilization, which are critical to the development of next-generation nuclear reactors. Ceramic materials with the hollandite structure $Ba_x(Mn^{4+}Mn^{3+})O_{16}$ reported by Byström in 1950 [1] have since garnered attention because of the potential use as one-dimensional ionic conductors [2, 3] and hosts for immobilization of radioactive cesium [4, 5], owing to their remarkable radiation resistance, crystal structure, chemical durability, and high thermodynamic stability [6–10].

The hollandite structure, generally expressed as $A_xB_8O_{16}$, consists of corner sharing $(B,Ti)O_6$ octahedra (e.g., B = Mg, Al and Ti), which form a framework with one-dimensional tunnels, along which the A cations (e.g., Na, K, and Cs) reside [11]. The $A_xB_8O_{16}$ unit cell and symmetry allow two positions for the A cations, but the structure is known to accommodate partially occupied A-site, i.e., $0 \leq x \leq 2$. The symmetry of hollandite can be either tetragonal (I4/m) with the tunnels along the c-axis or monoclinic (I2/m) with the tunnels along the b-axis [12].

Ceramic materials based on the hollandite structure have been studied for the development of crystalline matrices intended for the incorporation of radioactive cesium. In this context, several studies have showed thermodynamic stability in hollandite systems used for nuclear waste immobilization can be correlated to chemical durability and used to control (reduce) the release of mobile cations from the hollandite material [5, 7, 8, 13, 14]. In other applications such as solid-state batteries, the objective is not to immobilize certain elements, but rather the opposite, to increase their mobility. For example, the hollandite $K_{1.54}Mg_{0.77}Ti_{7.23}O_{16}$ first reported by Bernasconi et al. [2] and Beyeler et al. [3] exhibited an ionic conductivity (~ 10^{-2} S cm^{-1}). More recent research has provided further evidence that the structure of hollandites, specifically the corner sharing framework units, is more susceptible to localized distortions, which lower the energy barrier for conduction of the mobile cations in the tunnel. The current study explored the effects of varying K^+

✉ Kyle S. Brinkman
ksbrink@clemson.edu

1 Department of Materials Science and Engineering, Clemson University, Clemson, SC 29634, USA

2 Department of Mechanical Engineering, University of South Carolina, Columbia, SC 29208, USA

3 Savannah River National Laboratory, Aiken, SC 29808, USA

4 Department of Materials Science and Engineering, University of Michigan, Ann Harbor, MI 48109, USA

Published online: 12 February 2024

concentration and related to the structure, thermodynamic stability, and ionic conductivity as a function of occupancy of hollandite materials to gain a better understanding of the hollandite material properties for various applications.

Experimental methods

The $K_xMg_{x/2}Ti_{8-x/2}O_{16}$ ($1.54 \leq x \leq 2$) materials were synthesized using a solid-state reaction route. Reagent-grade powders of K_2CO_3, MgO, and TiO_2 were thoroughly mixed in stoichiometric proportions in a high-density polyethylene jar with zirconia grinding media and ethanol as solvent and ball milled for 24 h. The dried precursors were ground, pelletized, and calcined at 1000 °C for 5 h. The calcined powder was cold pressed into pellets and sintered. During heat treatment processes, alumina crucibles were covered with lids and sealed with cement to reduce the vaporization of K at high temperatures. Additional experimental details are contained in the supplementary information.

Results and discussion

Hollandite materials were synthesized with the general formula $K_xMg_{x/2}Ti_{8-x/2}O_{16}$ ($1.54 \leq x \leq 2$). Table 1 shows target and measured chemical composition of the hollandite phase. Differences observed between the target and measured concentrations are within the expected error and considered generally insignificant. There did appear to be measurable potassium loss, which was attributed to the volatility of potassium during calcination and sintering similar to prior reports [15]. Figure S1 shows XRD patterns of the sintered hollandite ceramics synthesized via solid-state route. The powder patterns for $K_xMg_{x/2}O_{16}$ correspond to ICDD-PDF# 84-0974 with specific (*hkl*) indices as shown. Inset image presents the lattice plane shifts for the primary peak (27.8°) of the samples, which demonstrates unit cell volume change as a function of the oxide framework. As observed in Fig. S1, all samples are major hollandite phases, suggesting the desired hollandite phase was formed. The 2θ angle of the most intense diffraction peak progressively shifts toward higher 2θ corresponding to a smaller interplanar spacing. When potassium ions are added into the tunnel, the attractive electrostatic interaction between the positive K ions and negatively charged O ions in the crystal lattice will cause a decrease in the interplanar spacing resulting in lattice contraction [16]. DFT calculations with the experimental values of composition from this study exhibited the same contraction of the lattice parameters ($a=b$) which were experimentally observed. Additionally, the lattice parameter c slightly increases with an increase in the potassium (K^+) content in the tunnels.

To gain detained insight into the microstructure of the hollandite, the characterization of the SK2 sample was conducted using STEM. Figure 1 presents the characteristic of a typical 2×2 tunnel of hollandite along the c-axis of tetragonal hollandite. The K^+ ions are situated at the center of the tunnel columns, while Mg^{2+} and Ti^{4+} ions form a square arrangement. The intensity contrast observed using STEM-HAADF is directly proportional to the average Z number in

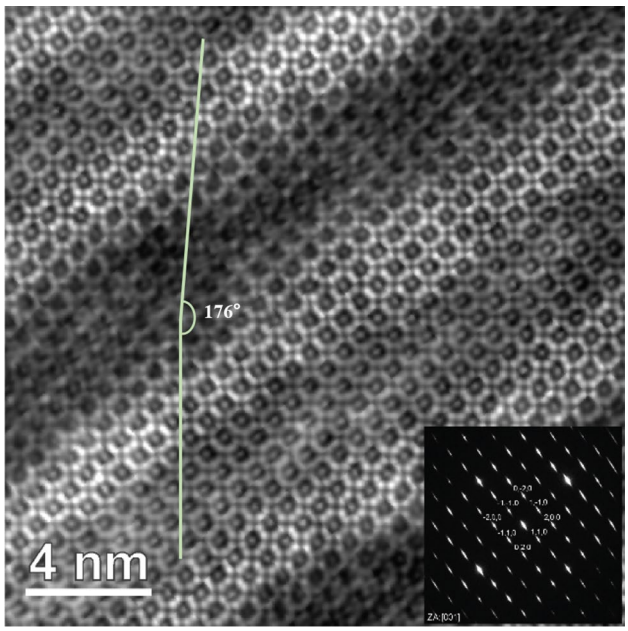

Fig. 1 The STEM-HAADF image and the corresponding electron diffraction pattern of the SSR-K2 along the [001] zone

Table 1 Sample identification, target composition, measured composition, space group, and lattice parameters of the $K_xMg_{x/2}Ti_{8-x/2}O_{16}$ hollandite samples

Sample	Target composition	Measured composition	Space group	$a=b$ (Å)	c (Å)	β (°)	V_{cell} (Å^3)
SK154	$K_{1.54}Mg_{0.77}Ti_{7.23}O_{16}$	$K_{1.49}Mg_{0.753}Ti_{7.279}O_{16}$	*I4/m*	10.1554(6)	2.97007(4)	90	306.309
SK160	$K_{1.60}Mg_{0.80}Ti_{7.20}O_{16}$	$K_{1.533}Mg_{0.785}Ti_{7.241}O_{16}$	*I4/m*	10.1524(6)	2.97091(3)	90	306.214
SK175	$K_{1.75}Mg_{0.88}Ti_{7.13}O_{16}$	$K_{1.625}Mg_{0.845}Ti_{7.17}O_{16}$	*I4/m*	10.1478(7)	2.97331(4)	90	306.187
SK2	$K_2Mg_1Ti_7O_{16}$	$K_{1.627}Mg_{0.991}Ti_{7.143}O_{16}$	*I4/m*	10.1425(3)	2.97457(6)	90	305.996

Numbers in parentheses are uncertainties in the last significant digit

the column. Thus, the Mg^{2+} and Ti^{4+} appear as a brighter feature than K^{+}. Furthermore, the measured lattice parameter of SK2 is 0.102 nm and aligns well with those listed in Table 1 for the structures.

The formation of superstructure in hollandites is often supported by the existence of satellite reflections in electron diffraction patterns. Previous studies have shown that compositional modulation for these superstructures is caused by tunnel-ion ordering [17]. Figure 1 exhibits a slight lattice rotation (~4°), accompanied by satellite reflections observed in the SAED pattern along the [001] zone axis of the sample. The rotation is attributed to a slight deviation from the original position of the tunnel site, resulting a positional disordering of tunnel cations [18].

The enthalpy of drop solution (ΔH_{ds}) of K-Mg-hollandite samples was measured using high-temperature oxide melt solution calorimetry (AlexSys 1000) in sodium molybdate solvent at 804 °C. An appropriate thermochemical cycle (Table S1) was used to calculate the formation enthalpies from the oxides ($\Delta H_{f,ox}$) at 25 °C using the measured enthalpies of drop solution (ΔH_{ds}) for the samples and constituent binary oxides. The enthalpies of drop solution for the samples as well as the enthalpies from the oxides are summarized in Table 2. The drop solution enthalpy (ΔH_{ds}) K_2CO_3 was measured in this work since it had not been previously measured at 800 °C but was needed for thermochemical calculations.

Figure 2 shows the enthalpy of formation of $K_xMg_{x/2}Ti_{8-x/2}O_{16}$ as a function of potassium content. The enthalpy of formation from the oxides becomes more negative with increasing potassium content and as the A-site becomes more occupied, as has been noted before for Cs-bearing hollandites [14]. This implies that increased potassium content in the A-site with titanium and magnesium on the B-site improves thermodynamic stability. For K-Ga titanate hollandite [19], the enthalpies of formation from the oxides were less exothermic than K-Mg titanate hollandite. This can be attributed to the smaller radius of Ga^{3+} (0.620 Å) than Mg^{2+} (0.720 Å) for sixth-fold coordination [19]. The experimental data are consistent with the density functional theory (DFT) simulations (see Fig. 2).

Table 2 Mean (ΔH_{ds}) drop solution enthalpies and formation enthalpies from the oxides at 25 °C synthesized via solid-state route

Analyzed sample composition	Mean ΔH_{ds} (kJ/mol)	$\Delta H_{f,ox}$ (kJ/mol)
$K_{1.49}Mg_{0.753}Ti_{7.279}O_{16}$	591.61 ± 2.86	− 269.93 ± 2.87
$K_{1.533}Mg_{0.785}Ti_{7.241}O_{16}$	598.27 ± 3.25	− 285.59 ± 3.25
$K_{1.625}Mg_{0.845}Ti_{7.17}O_{16}$	600.35 ± 3.50	− 306.17 ± 3.50
$K_{1.627}Mg_{0.991}Ti_{7.143}O_{16}$	597.71 ± 4.03	− 305.91 ± 5.24

*The errors reported in Table 2 were calculated as two standard deviations of the mean

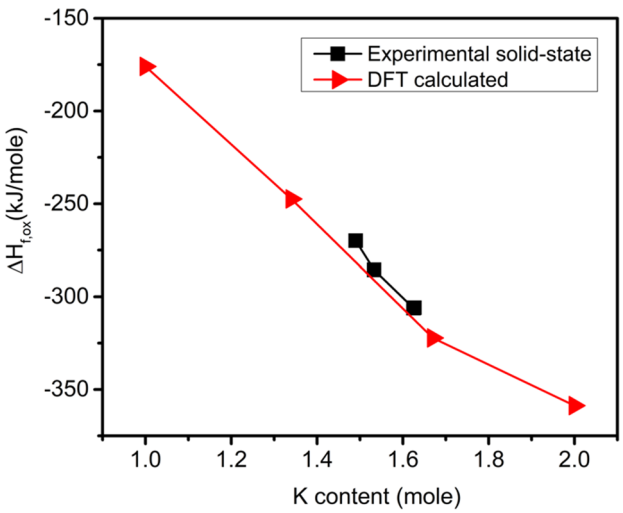

Fig. 2 Experimental enthalpies of formation from the oxides and DFT predictions for $K_xMg_{x/2}Ti_{8-x/2}O_{16}$ hollandite samples versus K content (x)

The IS spectra were used to determine the conductivity of $K_xMg_{x/2}Ti_{8-x/2}O_{16}$ hollandite with varying potassium content. Figure 3 shows the impedance plot for K-hollandite samples at 600 °C fitted with an equivalent circuit. In these models, R_g, R_{gb}, *and* $R_b + R_{gb}$ signify the grain (bulk), grain boundary, and sum of bulk and grain boundary resistance, respectively. Furthermore, R_s, R_e, and CPE represent series resistance, electrode resistance, and constant phase element, respectively. The results obtained from the circuit fitting indicated the resistivity increased with decreasing potassium content for the series of hollandite samples. The highest conductivity values were shown at 800 °C (highest temperature measured). Among all the samples, the highest conductivity of 1.0×10^{-4} S cm^{-1} was obtained from the sample with low K ions concentration ($K_{1.49}Mg_{0.753}Ti_{7.279}O_{16}$) whereas the sample with the highest K ion concentration (($K_{1.627}Mg_{0.991}Ti_{7.143}O_{16}$) of 5.4×10^{-5} S cm^{-1} at 800 °C exhibited the lowest conductivity of all the samples. As the potassium ion content increased, there was a decrease observed in the conductivity. Arrhenius plots of the total conductivity of $K_xMg_{x/2}Ti_{8-x/2}O_{16}$ ($1.54x \leq 2$) as a function of temperature are presented in Fig. 3 resulting in activation energies of 0.37 eV to 0.44 eV. The values obtained for activation energies are slightly higher than the previous results [20]. This can potentially be attributed to the change in x in $K_xMg_{x/2}Ti_{8-x/2}O_{16}$ due to potassium volatility during processing.

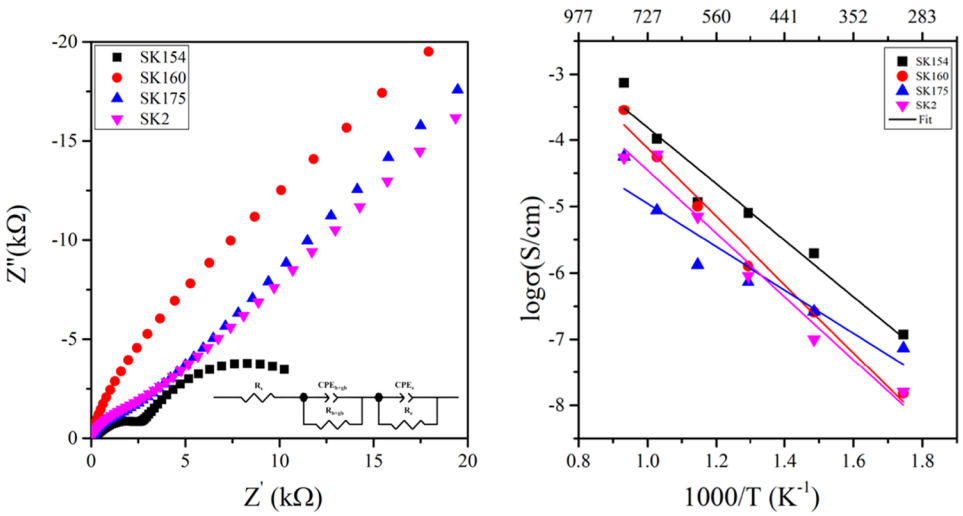

Fig. 3 (left) Complex impedance plots and inset representing equivalent circuit for $K_xMg_{x/2}Ti_{8-x/2}O_{16}$ ($x=1.54$) measured in air at 600 °C. R_s, R_{b+gb}, R_e, and CPE denote series resistance, sum of bulk and grain boundary resistance, electrode resistance, and constant phase element, respectively. (right) Arrhenius plot of total conductivity of $K_xMg_{x/2}Ti_{8-x/2}O_{16}$

Summary

Hollandite materials of the general formula $K_xMg_{x/2}Ti_{8-x/2}O_{16}$ ($1.54 \leq x \leq 2$) were obtained using the conventional solid-state method to study the correlation between varying potassium ion concentration on the hollandite structure, thermodynamic stability, and ionic conductivity. The thermodynamic stability of $K_xMg_{x/2}Ti_{8-x/2}O_{16}$ with varying potassium content was evaluated for the first time using high-temperature oxide melt solution calorimetry. The calorimetry results suggested that the hollandite composition with higher potassium content showed greater thermodynamic stability. Further analysis on structure property relations in tunnel structured systems is expected to enhance the understanding of the links between structure, thermodynamic stability, and physical properties such as ionic conductivity and corrosion/leaching behavior.

Supplementary Information The online version contains supplementary material available at https://doi.org/10.1557/s43580-024-00790-8.

Author contributions N.S.C was the first author performing material synthesis and calorimetry. S.J assisted with chemical synthesis, A.K.M assisted with conductivity measurements, N.B.coordinated calorimetry, and A.M.M. performed DFT under supervision of T.M.B. Y.L. performed TEM under supervision of L.W. J.WA. provided technical guidance and feedback on key points of manuscript and K.S.B managed, directed, and conceived of the work.

Funding The authors acknowledge support of the Center for Hierarchical Waste Form Materials, an Energy Frontier Research Center funded by the U.S. Department of Energy, Office of Science, Basic Energy Sciences (DE-SC0016574).

Data availability Data available upon reasonable request.

Declarations

Conflict of interest On behalf of all authors, the corresponding author states that there is no conflict of interest.

References

1. A. Byström, A.M. Byström, The crystal structure of hollandite, the related manganese oxide minerals, and α-MnO_2. Acta Crystallogr. **3**(2), 146–154 (1950). https://doi.org/10.1107/S0365110X500003 2X
2. J. Bernasconi, H.U. Beyeler, S. Strässler, S. Alexander, Anomalous frequency-dependent conductivity in disordered one-dimensional systems. Phys. Rev. Lett. **42**(13), 819 (1979). https://doi.org/10.1103/PhysRevLett.42.819
3. H.U. Beyeler, Cationic short-range order in the hollandite $K_{1.54}Mg_{0.77}T_{7.23}O_{16}$: Evidence for the importance of ion-ion interactions in superionic conductors. Phys. Rev. Lett. **37**(23), 1557 (1976). https://doi.org/10.1103/PhysRevLett.37.1557
4. A.E. Ringwood, S.E. Kesson, N.G. Ware, W. Hibberson, A. Major, Immobilisation of high-level nuclear reactor wastes in SYNROC. Nature **278**(5701), 219–223 (1979). https://doi.org/10.1038/278219a0
5. P. Tumurugoti, B.M. Clark, D.J. Edwards, J. Amoroso, S.K. Sundaram, Cesium incorporation in hollandite-rich multiphasic

ceramic waste forms. J. Solid-State Chem. **246**, 107–112 (2017). https://doi.org/10.1016/j.jssc.2016.11.007
6. M. Zhao, Xu. Yun, L. Shuller-Nickles, J. Amoroso, A.I. Frenkel, Y. Li, W. Gong, K. Lilova, A. Navrotsky, K.S. Brinkman, Compositional control of radionuclide retention in hollandite-based ceramic waste forms for Cs-immobilization. J. Am. Ceram. Soc. **102**(7), 4314–4324 (2019). https://doi.org/10.1111/jace.16258
7. W.J. Weber, A. Navrotsky, S. Stefanovsky, E.R. Vance, E. Vernaz, Materials science of high-level nuclear waste immobilization. MRS Bull. **34**(1), 46–53 (2009). https://doi.org/10.1557/mrs2009.12
8. M. Tang, P. Tumurugoti, B. Clark, S.K. Sundaram, J. Amoroso, J. Marra, C. Sun, P. Lu, Y. Wang, Y.-B. Jiang, Heavy ion irradiations on synthetic hollandite-type materials: $Ba_{1.0}Cs_{0.3}A_{2.3}Ti_{5.7}O_{16}$ (A= Cr, Fe, Al). J. Solid State Chem. **239**, 58–63 (2016). https://doi.org/10.1016/j.jssc.2016.04.014
9. G.C.C. Costa, H. Xu, A. Navrotsky, Thermochemistry of barium hollandites. J. Am. Ceram. Soc. **96**(5), 1554–1561 (2013). https://doi.org/10.1111/jace.12224
10. A.Y. Leinekugel-le-Cocq-Errien, P. Deniard, S. Jobic, E. Gautier, M. Evain, V. Aubin, F. Bart, Structural characterization of the hollandite host lattice for the confinement of radioactive cesium: Quantification of the amorphous phase taking into account the incommensurate modulated character of the crystallized part. J. Solid State Chem. **180**(1), 322–330 (2007). https://doi.org/10.1016/j.jssc.2006.10.013
11. R.W. Cheary, An analysis of the structural characteristics of hollandite compounds. Acta Crystallogr. Sect. B: Struct. Sci. **42**(3), 229–236 (1986). https://doi.org/10.1107/S0108768186098294
12. J.E. Post, R.B. Von Dreele, P.R. Buseck, Symmetry and cation displacements in hollandites: Structure refinements of hollandite, cryptomelane and priderite. Acta Crystallogr. Sect. B: Struct. Crystallogr. Cryst. Chem. **38**(4), 1056–1065 (1982). https://doi.org/10.1107/S0567740882004968
13. Y. Xu, Y. Wen, R. Grote, J. Amoroso, L.S. Nickles, K.S. Brinkman, A-site compositional effects in Ga-doped hollandite materials of the form $Ba_xCs_yGa_{2x+y}Ti_{8-2x-y}O_{16}$: Implications for Cs immobilization in crystalline ceramic waste forms. Sci. Rep. **6**(1), 1–8 (2016). https://doi.org/10.1038/srep27412
14. M. Zhao, N. Birkner, J. Schaeperkoetter, R.J. Koch, P. Russell, S.T. Misture, T. Besmann, J. Amoroso, K.S. Brinkman, Durable Cr-substituted $(Ba, Cs)_{1.33}(Cr, Ti)_8O_{16}$ hollandite waste forms with high Cs loading. J. Am. Ceram. Soc. **105**(6), 4564–4576 (2022). https://doi.org/10.1111/jace.18419
15. Z. Zhang, Y. Shao, B. Lotsch, Y.-S. Hu, H. Li, J. Janek, L.F. Nazar et al., New horizons for inorganic solid state ion conductors. Energy Environ. Sci. **11**(8), 1945–1976 (2018)
16. Q. Ding, W. Zheng, A. Zhao, Y. Zhao, K. Chen, X. Zhou, H. Zhang et al., W-doping induced efficient tunnel-to-layered structure transformation of $Na_{0.44}Mn_{1-x}W_xO_2$: Phase evolution, sodium-storage properties, and moisture stability. Adv. Energy Mater. (2023). https://doi.org/10.1002/aenm.202203802
17. M.L. Carter, R.L. Withers, A universally applicable composite modulated structure approach to ordered $Ba_xM_yTi_{8-y}O_{16}$ hollandite-type solid solutions. J. Solid State Chem. **178**(6), 1903–1914 (2005). https://doi.org/10.1016/j.jssc.2005.03.040
18. V. Aubin-Chevaldonnet, D. Caurant, A. Dannoux, D. Gourier, T. Charpentier, L. Mazerolles, T. Advocat, Preparation and characterization of (Ba, Cs)(M, Ti)$_8O_{16}$ (M= Al3+, Fe3+, Ga3+, Cr3+, Sc3+, Mg2+) hollandite ceramics developed for radioactive cesium immobilization. J. Nucl. Mater. **366**(1–2), 137–160 (2007). https://doi.org/10.1016/j.jnucmat.2006.12.051
19. M. Zhao, An investigation of structure, thermochemistry, electrochemistry, and stability of tunnel structured hollandite materials. PhD diss., Clemson University (2021)
20. J. Shao, J. Zheng, L. Qin, S. Zhang, Y. Ren, Wu. Yiying, K3SbS4 as a potassium superionic conductor with low activation energy for K-S batteries. Angew. Chem. **134**(20), e202200606 (2022). https://doi.org/10.1002/ange.202200606